

A simple microscopic description of quantum Hall transition without Landau levels

V. V. Mkhitarian¹, V. Kagalovsky², and M. E. Raikh¹

¹ *Department of Physics, University of Utah, Salt Lake City, UT 84112, USA*

² *Sami Shamoon College of Engineering, Beer Sheva 84100, Israel*

By restricting the motion of high-mobility 2D electron gas to a network of channels with smooth confinement, we were able to trace, both classically and quantum-mechanically, the interplay of backscattering, and of the bending action of a weak magnetic field. Backscattering limits the mobility, while bending initiates quantization of the Hall conductivity. We demonstrate that, in restricted geometry, electron motion reduces to *two* Chalker-Coddington networks, with *opposite* directions of propagation along the links, which are weakly coupled by disorder. Interplay of backscattering and bending results in the quantum Hall transition in a *non-quantizing* magnetic field, which decreases with increasing mobility. This is in accord with scenario of floating up delocalized states.

PACS numbers: 72.15.Rn; 73.20.Fz; 73.43.-f

Introduction. Quantization of the Hall conductivity of a disordered 2D electron gas, $\sigma_{xy} = n$, (in the units of e^2/h) together with vanishing diagonal conductivity, σ_{xx} , reflect the fact that in a perpendicular magnetic field delocalized states always constitute a discrete set [1].

In a strong magnetic field, $\omega_c\tau \gg 1$, where ω_c is a cyclotron frequency and τ is the scattering time, energy positions, E_n , of the delocalized states coincide with the centers of well-resolved Landau bands. Such a strong-field limit was the focus of theoretical studies of delocalization in a magnetic field. Most appealing qualitative picture [2] assumes a smooth disorder when the eigenstates are well-defined Larmor circles drifting along equipotential lines. Then delocalization corresponds to the *classical* percolation threshold; localized states above E_n are closed drift trajectories executed, *e.g.*, clockwise, while the states below E_n are closed drift trajectories executed counter-clockwise, see Fig. 1.

An alternative approach [3] to delocalization is based on renormalization-group equations, describing the evolution of σ_{xx} , σ_{xy} upon increasing the sample size, L ,

$$\frac{\partial \sigma_{xx}}{\partial \ln L} = -\frac{1}{2\pi^2 \sigma_{xx}} - \sigma_{xx}^2 D e^{-2\pi \sigma_{xx}} \cos(2\pi \sigma_{xy}), \quad (1)$$

$$\frac{\partial \sigma_{xy}}{\partial \ln L} = -\sigma_{xx}^2 D e^{-2\pi \sigma_{xx}} \sin(2\pi \sigma_{xy}), \quad (2)$$

where D is a dimensionless constant. First term of Eq. (1) originates from *interference* of electron multiple-scattering paths: two paths corresponding to the *same* scatterers but different sequences of scattering events interfere even in the presence of Aharonov-Bohm phases. Second term reflects the *orbital* action of magnetic field: by curving electron trajectories it tends to destroy the interference. When the “phase” and “orbital” terms compensate each other, delocalization transition takes place.

Field-theoretical approach [3] yields a highly nontrivial prediction first pointed out by Khmel'nitskii [4]. Namely, solving Eqs. (1), (2) together with classical initial condition $\sigma_{xy}(\omega_c) = \sigma_0 \omega_c \tau (1 + \omega_c^2 \tau^2)^{-1}$, where $\sigma_0 \propto E_n$ is the dimensionless conductance at $\omega_c = 0$, yields $E_n =$

$\hbar \omega_c (n + \frac{1}{2}) [1 + (\omega_c \tau)^{-2}]$. As shown in Fig. 1 for $n = 0$, the high-field part, $\omega_c \tau \gg 1$, of E_0 follows the center of the lowest Landau level, while the low-field part “floats up” as $\omega_c \tau \rightarrow 0$. This prediction is essential component of the global phase diagram [5].

Qualitative classical picture [2] applies to the high-field part and illustrates the restructuring, see Fig. 1, of the motion of guiding center, which accompanies the crossing of E_0 by the Fermi level, upon increasing magnetic field ($1 \rightarrow 0$ transition into the quantum Hall insulator [6]).

While there is certain experimental evidence [7, 8, 9, 10, 11, 12, 13] that floating up of $E_0(\omega_c)$ indeed takes place, tight-binding numerical studies [14, 15, 16] are less conclusive. There is a fundamental reason [17] for this lack of conclusiveness. Indeed, significant floating up occurs for large $\sigma_0 > (\omega_c \tau)^{-1} \gg 1$. For such σ_0 , upon moving along the dashed horizontal line in Fig. 1 the localization length undergoes a steep growth from orthogonal value $\xi_o \sim \exp(\pi \sigma_0)$ to the unitary value $\xi_u \sim \exp(\pi^2 \sigma_0^2)$ already in very small fields $\omega_c \tau \simeq \sigma_0^{-1} e^{-2\pi \sigma_0}$, way before the expected transition at point L . Such large ξ_u is a major obstacle for numerics to capture the descending region of the line of transitions in Fig. 1. Accessing this region

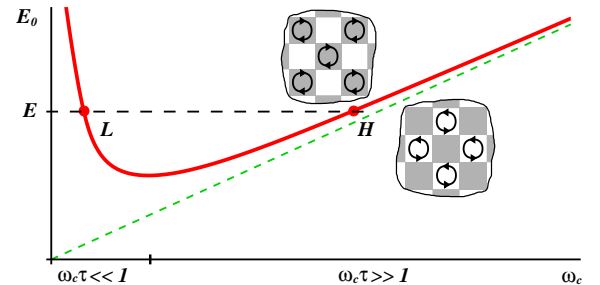


FIG. 1: (Color online) Energy position of the lowest delocalized state, E_0 , vs. magnetic field, ω_c , as predicted in Ref. 4. For a given E , delocalization transition occurs at points L and H . Change of character of electron motion near H is illustrated schematically. Corresponding change near L is illustrated in Fig. 5 (a \leftrightarrow e).

requires to construct an efficient minimal description of a weak-field transition, as transparent as the picture [2] sketched near the point H in Fig. 1. This goal is achieved in the present paper. The key step of our construction is separation of the spatial regions with disorder-induced scattering and field-induced bending.

Restricted electron motion. (i) In contrast to unidirectional motion in strong fields, we allow counter-propagating paths in the regions where *orbital* action of magnetic field is negligible. We achieve this by restricting electrons to narrow point contacts, see Fig. 2. At the same time, we assume that the *phase* action of magnetic field is well-developed in each point contact, i.e., the area of the contact is threaded by many flux quanta. Presence of disorder is incorporated by allowing mutual backscattering of two counterpropagating waves. We quantify the strength of backscattering with probability, p , so that the scattering matrix of the contact has the form

$$\begin{pmatrix} Z_1 \\ \tilde{Z}_2 \end{pmatrix} = \begin{pmatrix} \sqrt{1-p} & \sqrt{p} \\ -\sqrt{p} & \sqrt{1-p} \end{pmatrix} \begin{pmatrix} \tilde{Z}_1 \\ Z_2 \end{pmatrix}, \quad (3)$$

with amplitudes Z_i, \tilde{Z}_i , Fig. 2, having random phases.

(ii) The orbital action of magnetic field takes place in the junctions between the point contacts, Fig. 2. To simplify the description of the junction, we assume that an electron incident, say, from the left, after several bounces [18] off the walls exits either “up” or “down”, i.e., both forward and backward scattering channels are suppressed. This assumption allows us to quantify the bending strength of the junction by a single parameter, q , the deflection probability to the right, Fig. 2. Then the deflection probability to the left is $(1 - q)$. The Hall resistivity of the junction [18] is then given by $R_H = (e^2/h)[q - (1 - q)]/[q^2 + (1 - q)^2]$, so that $q = 1/2$ corresponds to a zero field. Expression for the scattering matrix of the junction is the following

$$\begin{pmatrix} Z_2 \\ Z_4 \\ Z_6 \\ Z_8 \end{pmatrix} = \begin{pmatrix} 0 & \sqrt{1-q} & 0 & \sqrt{q} \\ \sqrt{q} & 0 & \sqrt{1-q} & 0 \\ 0 & -\sqrt{q} & 0 & \sqrt{1-q} \\ \sqrt{1-q} & 0 & -\sqrt{q} & 0 \end{pmatrix} \begin{pmatrix} Z_1 \\ Z_3 \\ Z_5 \\ Z_7 \end{pmatrix}. \quad (4)$$

With scattering matrices Eqs. (3), (4) defined, the problem of electron localization by disorder in a magnetic field reduces to the effective network model, which can be studied by transfer-matrix method, similar to Chalker-Coddington (CC) model [19], which describes delocalization transition at the point H in Fig. 1. As in Ref. 19, “unitary” disorder is incorporated via random phases of the link amplitudes, Z_i . Delocalization transitions in the network define a line on the (p, q) plane. Important is that this line can be converted into the dependence $E_0(\omega_c)$. Indeed, parameter q reflects the strength of magnetic field, so that $(\frac{1}{2} - q) \propto \omega_c$, while the backscattering probability, p , decreases monotonously with increasing energy. Thus, the floating scenario is equivalent to

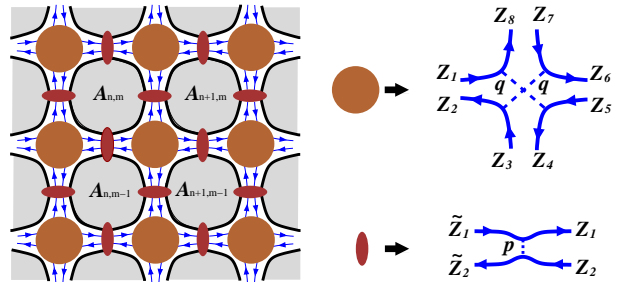


FIG. 2: (Color online) Left: Restricted electron motion over point contacts and bend-junctions is illustrated; $A_{n,m}$ are the centers of forbidden regions. Right: Scattering matrices of the junction and of the point contact.

the statement that $p(q)$ -line approaches $p = 0$ as q approaches $\frac{1}{2}$. Below we argue that the form of $p(q)$ -line of delocalization transitions is the one shown in Fig. 3(a) (region $q < \frac{1}{2}$), so that it indeed yields the dependence, $p(q)$, corresponding to the floating of $E_0(\omega_c)$.

In the CC model the transmission of the nodes with “height”, E_i , and “width”, Γ , is given by the Fermi function [20] $T(E, E_i) = \{1 + \exp[(E_i - E)/\Gamma]\}^{-1}$. Qualitative strong-field picture of the transition [2] emerges when the spread, W , of heights, E_i , is $\gg \Gamma$. Then the quantum interference can be neglected up to large distances, $\mathcal{R}_{cl} = (W/\Gamma)^{4/3} \gg 1$, determined by the classical percolation. For smaller distances, one can replace $T(E, E_i)$ by a step-function, $\Theta(E_i - E)$. Adopting the same approach, we assume that (i) in Fig. 2 full transmission takes place in p percent of point contacts, and full reflection in the rest $(1 - p)$ percent; (ii) a given junction deflects only to the left in q^2 percent of cases, only to the right in $(1 - q)^2$ percent of cases; in the remaining $2q(1 - q)$ percent the deflection takes place both to the left and to the right depending on incoming channel.

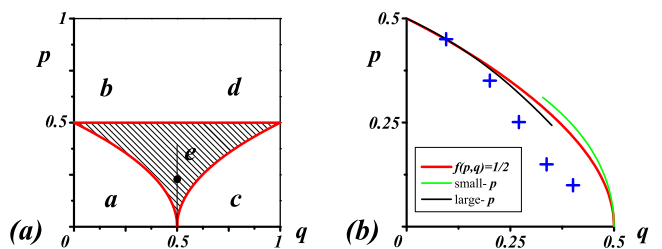


FIG. 3: (Color online) (a) Classical metallic phase, dashed region (e) in the (p, q) -plane separates different insulating phases of the model Fig. 2; (b) Line of classical delocalization transitions in the (p, q) -plane. Asymptotes Eqs. (??), (6), are shown with green and black lines, respectively; red curve interpolates between the two regimes. Crosses show the positions of quantum delocalization transition inferred from simulations for five values of “energies”, p . Quantized σ_{xy} is 1 in phase (a), -1 in phase (c), and 0 in (b), (d), and (e).

Phase diagram. The key observation that allows to establish the phase diagram Fig. 3 is that the classical electron motion over the lattice of point contacts and junctions can be reduced to a single problem of *joint* bond percolation over “p” and “q” -bonds. To substantiate this statement, we focus on the grey squares in Fig. 2, which are “forbidden” regions for electrons, and notice that electron scattering processes *both* in point contacts and junctions effectively establish bonds between these regions. More specifically, if electron is backscattered in a point contact, we consider that the *centers* $A_{n,m}$ and $A_{n,m-1}$ of the squares, adjacent to this contact, are connected by a bond, see Fig. 4. Further, if electron is bent-scattered by a junction, say, in the direction left \rightarrow down, we identify this process with establishing a bond between the centers of the squares $A_{n,m}$ and $A_{n-1,m-1}$. The above identification reduces the classical motion through the network with sites in the centers of squares, see Fig. 4.

Structure of phases. We start from the region of strong reflection, $p > \frac{1}{2}$. Counterpropagating channels in point contacts, Fig. 2, are essentially “short-circuited”. Hence, no delocalization occurs upon increasing magnetic field, $(\frac{1}{2} - q)$. Localized states are illustrated schematically in Fig. 5 in the limit $(1 - p) \ll 1$. It is apparent that crossover from clockwise rotation (b) to counterclockwise rotation (d) upon passing the zero-field line $q = \frac{1}{2}$ takes place without delocalization. This absence of delocalization is consistent with low-energy part of Fig. 1, because $p > \frac{1}{2}$ corresponds to small σ_0 . Along the line $p = \frac{1}{2}$ the p -bonds alone constitute a critical network. It is seen from Fig. 5 that, as p is reduced below $\frac{1}{2}$, q -bonds sustain percolation, manifesting that metallic behavior for $\sigma_0 > 1$ persists up to strong magnetic fields, $\omega_c \tau \sim 1$.

We now turn to the most interesting region of small p (high energies in Fig. 1). In this domain the overall connectivity of the network is dominated by the q -bonds. Moreover, at $p = 0$ the light-blue and dark-blue subnetworks are *completely decoupled*. Small finite p becomes essential in the vicinity of $q = \frac{1}{2}$, when both subnetworks of q -bonds are critical. Now even weak non-zero p , by coupling the subnetworks, results in opening of a *metallic* region (e) in the phase diagram. This disorder-induced

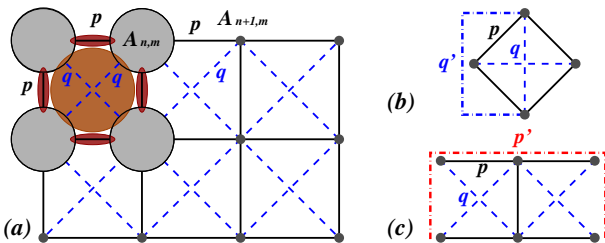


FIG. 4: (Color online) (a) In the classical limit, electron motion reduces to the bond percolation on the lattice consisting of p and q -bonds; (b) and (c) are graphic representation of Eqs. (??) and (6), respectively.

coupling of critical subnetworks is the fundamental underlying mechanism for the restructuring of states near the point L , Fig. 1. In effect, transformation (e) \rightarrow (a) with increasing field, $(\frac{1}{2} - q)$, is the counterpart of transformation near the point H in quantizing ω_c .

Fig. 5 (a) also illustrates that at small p both subnetworks are chiral. Transformation into the phase (e) upon decreasing magnetic field is accompanied by the change of the Hall conductivity from quantized to finite value smaller than 1. Full suppression of σ_{xy} in the region (e) occurs only when interference drives this region into the Anderson insulator, so that the difference between (e) and strongly localized phases (b) and (d) vanishes.

Calculation results for the phase boundaries are shown in Fig. 3(b) only for $q < \frac{1}{2}$ due to $q \rightarrow (1 - q)$ duality [21]. The end-points $(p, q) = (0, \frac{1}{2})$ and $(p, q) = (\frac{1}{2}, 0)$ are conventional bond percolation thresholds for percolation over regions $A_{m,n}$, connected by q -bonds and by p -bonds, respectively, see Fig. 4. Next, consider small $p \ll 1$ and suppose that q is slightly smaller than $\frac{1}{2}$. Then, instead of missing q -bond, a *pair of one horizontal and one vertical* p -bonds can provide the connection (there are two such variants, see Fig. 4b). Resulting shift of the threshold position is determined by the condition

$$f(p, q) = q' = q + 2(1 - q)p^2(1 + q) = 1/2, \quad (5)$$

where q' is the probability that effective q -bond connects.

When q is small, the role of q -bonds is to promote percolation over p -bonds. Unlike the previous case, the shift, $(\frac{1}{2} - p)$, of the threshold is *linear* in q . This is because in certain rare cases *one* q -bond takes on the role of a missing p -bond. Assume that a vertical p -bond is absent while one of the neighboring horizontal p -bonds is present. Then the connection between the ends of the missing bond can be established in two

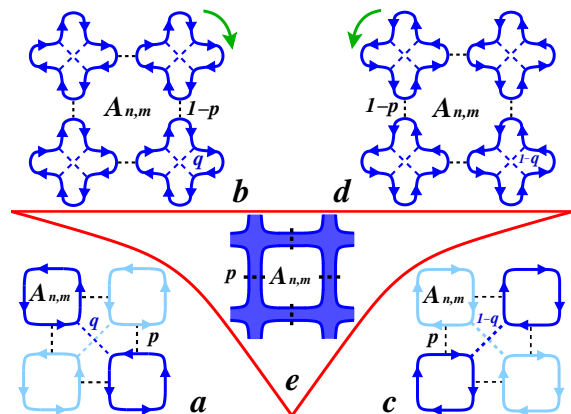


FIG. 5: (Color online) Illustration of the structure of five different phases in Fig. 3. Electron moves predominantly along solid directed lines. In phases a and c the motion is either within dark or within light subnetwork. In phase e coupling of subnetworks by p -bonds opens a metallic phase.

steps: first via this horizontal p -bond and then via a q -bond, Fig. 4. Quantitatively, the boundary $p(q)$ at small q can be obtained from the real-space renormalization group procedure [22]. In Ref. 22 the probability that the superbond, illustrated in Fig. 4c connects, is given by $f_0(p) = p^5 + 5p^4(1-p) + 8p^3(1-p)^2 + 2p^2(1-p)^3$, where the last three terms correspond to realizations when superbond connects with one, two, and three original bonds removed; $f_0(p) = \frac{1}{2}$ yields the exact threshold $p = \frac{1}{2}$. Using the fact that q -bonds can restore the connectivity, and selecting suitable realizations out of all 2^4 possible states of q -bonds amounts to the following modification of the probability, $p' = f(p, q)$, that superbond connects

$$f(p, q) = f_0(p) + 10p^2(1-p)^3[2q - q^2] + p(1-p)^4[4q + 8q^2 - 8q^3 + q^4] + (1-p)^5[2q^2 - q^4]. \quad (6)$$

Upon equating $f(p, q)$ to $\frac{1}{2}$, Eq. (6) yields the boundary of percolation transition at small q .

Localization length. The boundary a - e of “classical” phase diagram Fig. 3, is characterized by the critical exponent $\nu = \frac{4}{3}$. Simulations, see below, indicate that, with quantum interference, the phase diagram Fig. 3b remains unchanged, while metallic phase in Fig. 5e turns into the Anderson insulator with “unitary” localization length, $\ln \xi_u = \pi^2 \sigma_0^2$, where the Drude conductance is related to p as $p = c\sigma_0^{-1}$, with $c \sim 1$. Interference also modifies the divergence of the localization length

$$\xi(p, q) \sim |f(p, q) - 1/2|^{-\nu} = |3p^2/2 - (1/2 - q)|^{-\nu}, \quad (7)$$

in the neighboring insulating region, Fig. 5a, by changing ν from $\nu = \frac{4}{3}$, to quantum $\nu \approx \frac{7}{3}$. Starting from small field, $(\frac{1}{2} - q) \ll p^2$, ξ retains its value $\xi_u \propto \exp(\pi^2 c^2 / p^2)$ up to the narrow vicinity of the boundary, $(\frac{1}{2} - q) = \frac{3}{2}p^2$, when it crosses over to diverging Eq. (7). The width of the “quantum” region can be estimated as

$$\frac{\delta \omega_c}{\omega_c} = \frac{\delta(1/2 - q)}{(1/2 - q)} = \frac{1}{p^2} e^{-\frac{3c\pi^2}{7p^2}} = \frac{\sigma_0^2}{c^2} e^{-\frac{3}{7}\pi^2 \sigma_0^2}. \quad (8)$$

This region rapidly narrows in course of floating up.

Quantum treatment of the network. Numerical simulations, employing matrices Eqs. (3), (4) for nodes and incorporating random phases into the link amplitudes, are required to verify the above predictions based on the classical picture. They are also supposed to verify that domain (e) in Fig. 3 is, quantum-mechanically, insulating. The results of transfer-matrix analysis of the two-channel [23] network Fig. 2 are shown in Fig. 3b for five values of “energy”, p . Usual simulation procedure [24] was employed: upon constructing a transfer matrix of a slice (M nodes in transverse direction with periodic boundary conditions) the net transfer matrix of a system of length, N (typical $N = 240000$), was obtained and diagonalized, yielding the Lyapunov exponents, $\lambda_i(p, q)$, related to the eigenvalues as $\exp(\lambda_i N)$. Localization

length, $\xi_M(p, q)$, was inferred from the smallest positive exponent: $\xi_M(p, q) = \lambda_{M/2}^{-1}$. Simulation confidently confirm that for finite “energies”, $p > 0$, quantum system is insulating at $q = 0.5$, while the state with $p = 0$ and $q = 0.5$ is extended. As seen in Fig. 3b, the discrepancy between classical and quantum treatments is small.

Note in conclusion that among various network models studied [25], the closest to ours is the model [26]. Unlike Ref. 26 our Eq. (4) describes scattering, say, to the right, with the *same* probability,

Acknowledgments. This work was supported by the BSF grant No. 2006201.

-
- [1] B. I. Halperin, Phys. Rev. B **25**, 2185 (1982).
 - [2] R. F. Kazarinov and S. Luryi, Phys. Rev. B **43**, 7626 (1982); S. V. Iordansky, Solid State Commun. **43**, 1 (1982); S. A. Trugman, Phys. Rev. B **27**, 7539 (1983).
 - [3] A. M. M. Pruisken, Nucl. Phys. B **235**, [FS11], 277 (1984); A.M.M. Pruisken and I.S. Burmistrov, Ann. Phys. **316**, 285 (2005).
 - [4] D. E. Khmel'nitskii, Phys. Lett. **106A**, 182 (1984).
 - [5] S. Kivelson, D.-H. Lee, and S.-C. Zhang, Phys. Rev. B **46**, 2223 (1992).
 - [6] L. P. Pryadko and A. Auerbach, Phys. Rev. Lett. **82**, 1253 (1999); E. Shimshoni, Mod. Phys. Lett. B **18**, 923 (2004).
 - [7] H. W. Jiang et al., Phys. Rev. Lett. **71**, 1439 (1993).
 - [8] C. E. Johnson and H. W. Jiang, Phys. Rev. B **48**, 2823 (1993).
 - [9] T. Wang et al., Phys. Rev. Lett. **72**, 709 (1994).
 - [10] R. J. F. Hughes et al., J. Phys.: Condens. Matter **6**, 4763 (1994).
 - [11] I. Glazman, C. E. Johnson, and H. W. Jiang, Phys. Rev. Lett. **74**, 594 (1995).
 - [12] A. A. Shashkin, G. V. Kravchenko, and V. T. Dolgoplov, JETP Lett. **58**, 220 (1993).
 - [13] M. Hilke et al., Phys. Rev. B **56**, R15545 (1997).
 - [14] K. Yang and R. N. Bhatt, Phys. Rev. Lett. **76**, 1316 (1996).
 - [15] see D. N. Sheng, Z. Y. Weng, and X. G. Wen, Phys. Rev. B **64**, 165317 (2001), and references therein.
 - [16] Th. Koschny and L. Schweitzer, Phys. Rev. B **70**, 165301 (2004), and references therein.
 - [17] B. Huckestein, Phys. Rev. Lett. **84**, 3141 (2000).
 - [18] D. G. Ravenhall, H. W. Wyld, and R. L. Schult, Phys. Rev. Lett. **62**, 1780 (1989); H. U. Baranger and A. D. Stone, Phys. Rev. Lett. **63**, 414 (1989); C. W. Beenakker and H. van Houten, Phys. Rev. Lett. **63**, 1857 (1989).
 - [19] J. T. Chalker and P. D. Coddington, J. Phys. C **21**, 2665 (1988).
 - [20] H. A. Fertig and B. I. Halperin, Phys. Rev. B **36**, 7969 (1987).
 - [21] Due to this duality, quantized σ_{xy} in the phases (a) and (c) are equal to 1 and -1 , respectively. The easiest way to see that phase (a) possesses a single edge state is to notice that along the line $q = 0$ our model reduces to a *single* CC model with p-bonds acting as nodes.
 - [22] P. J. Reynolds, W. Klein, and H. E. Stanley, J. Phys. C **10**, L167 (1977).

- [23] V. Kagalovsky, B. Horovitz, and Y. Avishai, Phys. Rev. B **52**, R17044 (1995).
- [24] A. MacKinnon and B. Kramer, Phys. Rev. Lett. **47**, 1546 (1981).
- [25] B. Kramer, T. Ohtsuki, and S. Kettemann, Phys. Rep. **417**, 211 (2005).
- [26] M. Bocquet and J. T. Chalker, Phys. Rev. B **67**, 054204 (2003).